DISPERSION OF HEATED PARTICLES IN A SUBSONIC JET

Ahmed Saieed
Department of Mechanical and Mechatronics Engineering
University of Waterloo
200 University Ave W, Waterloo, Ontario N2L 3G1, Canada
asaieed@uwaterloo.ca

Jean-Pierre hickey
Department of Mechanical and Mechatronics Engineering
University of Waterloo
200 University Ave W, Waterloo, Ontario N2L 3G1, Canada
j6hickey@uwaterloo.ca

ABSTRACT

The clustering of heated particles is known to increase due to the rise in local gas viscosity, even when the particle Stokes number is less than unity. However, so far this rise in clustering has been only probed in a triply periodic box via direct numerical simulations (DNS), in which the flow evolves temporally and the total volume (and mean density) is fixed. In this regard, we conducted DNSs to study the dispersion of heated polydispersed particles in a subsonic confined jet flow. We modeled both energy and momentum with two-way coupling, and neglected the inter-particle collisions and gravitational force. Despite the fact that the thermodynamic difference between the heated and unheated simulations was minimal (only 16% increase in viscosity in the heating case), the rise in jet viscosity upon heating caused the particles to stay within the central region of the jet. On the other hand, the particles travelling laterally encountered a thermal front created at the outer periphery of the jet, and started clustering there. Thus, their lateral dispersion was also limited, and even the particle reaction force due to the two-way momentum coupling was not enough to oppose this phenomenon. As a result, despite starting with similar Stokes number values as their unheated counterparts, the concentration of heated particles sharply declines in the lateral direction. This is a compounding effect, where the presence of particles within the jet can produce more significant thermal changes inside the jet, which can further restrict the lateral movement of the particles. Also, this phenomenon caused heated particles to yield more concentrated clusters, which can also lead to higher viscosity-driven clustering. Experiencing identical large scale eddies inside the jet results in particles of all sizes in the heating case to depict clustering at similar locations in the domain. These findings can considerably aid applications such as targeted drug delivery and cold spray coating techniques.

Introduction

Heated particle-laden jets are frequently employed in applications such as powder metallurgy (Li *et al.*, 2020), thermal spray coatings (Herman & Sampath, 1996), and particle combustion in thrust generating engines (Hobosyan *et al.*, 2019). In particle-laden thermal system, the operational efficiency inherently relies on the uniform distribution of particles. However, particles intrinsically tend to cluster due to their inertia, which cause them to evade high vorticity regions and cluster in high strain rate regions based on the centrifugal force acting on the particles (Squires & Eaton, 1991). This phenomenon is referred to as *preferential concentration*, and is considered the leading cause of particle clustering. Such clustering is particularly problematic in thermal applications as it can decrease the particle-to-fluid heat transfer by up to 25% (Pouransari & Mani, 2017) and in combustion applications it can entirely impede combustion within a cluster (Rahman *et al.*, 2022). Therefore, a fundamental focus of such thermal applications is to avoid clustering.

In past literature, particle clustering has been mainly characterized with Stokes number St, where St is the ratio of particle momentum timescale (τ_p) to turbulence timescale (τ) (Crowe *et al.*, 1985). For τ, we use the convective timescale (τ_c) of the jet, which is similar to the large eddy timescale of the jet. Chung & Troutt (1988) reported that in a round jet, the particle dynamics is governed by the large scale structures of the flow. The convective timescale is the ratio of jet half-width ($r_{1/2}$) and centerline velocity (u_c). Thus, St is given as:

$$St = \frac{\rho_p d_p^2 u_c}{18 \rho_f \nu_f r_{1/2}} \tag{1}$$

In Equation (1), the subscripts f, p and j are used to define the fluid, particle and jet parameters, respectively. Additionally, d, ν and ρ are for diameter, fluid kinematic viscosity and density. Past research reach a consensus on the fact that, typically in unheated particle-laden jet flows, particles with $St \leq 1$ spread laterally and cluster at the outer periphery of the jet (Hardalupas *et al.*, 1989). The $St \gg 1$ particles travel and cluster at the centerline of the jet core (Lau & Nathan, 2014). The $St \approx 1$ particles, which are known for depicting maximum clustering in isotropic turbulence (Eaton & Fessler, 1994), can be completely pushed out of the jet by the large eddies (Chung & Troutt, 1988).

On the contrary, involvement of heat causes the fluid thermodynamic parameters to alter along with the kinematic variables. This is concerning as the two fundamental effects that are the decrease in local gas density and increase in viscosity due to particle heating can considerably modulate turbulence. Moreover, change in each of these variables influence particle clustering directly. The decrease in density in the vicinity of a cluster pushes particles away (enhances dispersion by creating a local diverging flow field) (Pouransari *et al.*, 2017). On the other hand, the rise in gas viscosity enhances clustering according to a phenomenon called *viscous capturing* (VC) (Saieed *et al.*, 2022; Saieed & Hickey, 2024). As per the VC effect, a large cluster rapidly increases the local gas temperature and viscosity. This high viscosity gas, termed as a *viscous cloud*, then offers higher drag to the particles it envelops, compared to the surrounding relatively cold fluid, promoting these particles to remain clustered. These viscous clouds also capture more particles in the domain. Hence, the overall particle clustering increases. In the flows where VC is present, maximum particle clustering can be observed at $St < 1$ instead of $St \approx 1$.

Considering the discussion above, it is essential to probe the effect of temperature-dependent viscosity on heated particle clustering dynamics in flows which are developing both temporally and spatially. This is crucial because in the previous studies, homogeneous isotropic turbulence (HIT) generated in a triply period box was used, in which the flow simply progresses temporally (Saieed *et al.*, 2022). Furthermore, in this case the gas does not undergo expansion as the volume of the domain is constant. In this regard, we opted for a heated particle-laden jet flow due to its significance in engineering applications, as stated earlier. For simplicity, we restrict this study to subsonic circular jets, while the added complexity arises from the two-way fluid-particle momentum and energy coupling, whereas inter-particles collisions are also neglected. Note that, although particles can oppose the force exerted on them by the fluid in two-way momentum coupling, enhanced clustering due to higher local gas viscosity was found to prevail over the particle reaction drag force (Saieed & Hickey, 2024, 2023). We hypothesize that in the present flow scenario, particles can be spatially restricted within the high viscosity regions, which can also lead to higher clustering. Note that the rise in gas viscosity is expected to be considerably smaller in the subsonic jet flow compared to the HIT case. This is because, here, particles only occupy a small portion of the domain. Also, the cold fluid continuously enters the domain at the inlet and the heated fluid leaves the domain at the outlet. To this end, we scrutinized the dispersion characteristics of heated polydispersed particles in a subsonic jet flow consisting of four different particle sizes, using DNS. The particle sizes were opted such that particles are small enough ($d_p \ll \eta$, where η is Kolmogorov length scale) to be modeled as point-particles, while simultaneously provide a sizeable range of St.

Methodology

In this analysis, we conducted DNS using an in-house version of an open source finite difference code, called Pencil-Code (Brandenburg *et al.*, 2020). Here, the point-particles and fluid are modeled with the Lagrangian and Eulerian schemes, respectively. As a first step, a DNS of a triply periodic box with characteristics length of $9d_j$ is carried out to generate turbulence (without particles) with the help of a solenoidal forcing function. This DNS box is resolved into a mesh of 256^3 cells. We sustained the forcing until the mean turbulence statistics stabilized, indicating the equilibrium state between the large

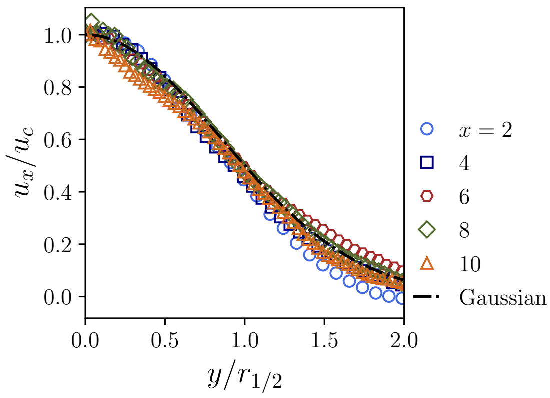

Figure 1. Normalized jet axial velocity (u_x) at five downstream locations, shown as a multiple of d_j.

scale energy addition and the small scale dissipation. At this stage, 3D snapshots of the mean velocity field are periodically projected at the inlet of a rectangular domain with $14 \times 9 \times 9d_j$ dimensions in the streamwise (x) and two lateral (y and z) directions. It should be noted that all the dimensions in this article are presented in terms of jet diameters, d_j, which is unity. This domain is prescribed with periodic boundary condition (BC) in y and z directions, while inflow and outflow BCs are set at its inlet and outlet, respectively. Spurious boundary reflections at the inlet (Lodato *et al.*, 2008) and outlet (Poinsot & Lelef, 1992) are minimized via *Navier-Stoke Characteristics Boundary Condition* (NSCBC). At the inlet, fluid was allowed to enter the domain only through a circular jet inlet of d_j with a mean velocity of $u_j = 1$ (inlet mach number is $M = 0.24$), and the rest of the inlet plane is a wall. The y and z walls should also have outflow BCs, however we used periodic BC at these walls, due to a limitation of our code where a discontinuity arises at the corners where walls meet.

We divided this rectangular box into a grid of $384 \times 256 \times 256$ cells in the x, y and z directions. This simulation is also carried out without particles, with the sole purpose of developing the jet. This jet is allowed to evolve for about 1.5 flows through time, such that its axial velocity and axial turbulent intensity ($u' = (\overline{u'^2})^{1/2}$) profiles become self-similar at the locations shown in Figures 1 and 2. In these figures, we observe that our trends reasonably overlap with the expected results, hence our simulation setup is acceptable for further analysis. Note that despite modeling a domain length of $x = 14$, we only presented data up to $x = 10$ in these figures to eliminate any imperfection arising from NSCBC at the outlet.

Once the jet development is ensured, we slowly introduced 100,000 particles during the 3.3 flows through time of these simulations. The considered particle loading density leads to a volume fraction of $O(10^{-6})$, which divides the one- and two-way momentum coupling regimes (Elghobashi, 1994). However, these particles are introduced within the jet diameter of $d_j = 1$, and a majority of these particles occupy the central region of the domain (as discussed in the next section). Therefore, two-way momentum coupling is employed in this study. Note that these particle simulations were carried out for roughly 3.3 flows through time in order for the flow statistics to stabilize. The entrained particles consist of four particle diameters that are $d_p = 0.001$, 0.003, 0.004 and 0.006 at the jet inlet. For brevity, we will denote these particle sizes with P1, P2, P3 and P4 from here onward. For introduction into the jet stream, these particles are given a random x velocity at the in-

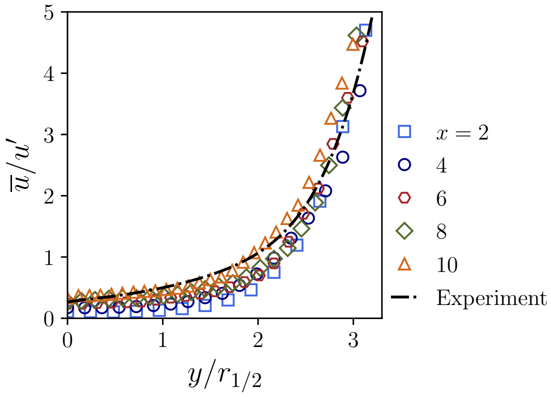

Figure 2. Axial turbulent intensity ($u' = (\overline{u'^2})^{1/2}$) normalized with the mean jet velocity ($\overline{u}$). The present radial profiles of u' are compared with the experimental data of Hussein *et al.* (1994), shown as "$-\cdot$" line.

let. To highlight the effect of particle heating on clustering, we run simulations with heating (**H**) and without heating (**NH**). For the above stated particle sizes, the *St* of the two simulations start with similar values of 0.6 (P1), 2 (P2), 5.1 (P3) and 10.4 (P4). The constant particle density is $\rho_p = 1500$, while their initial temperature is $T_{p,0} = 1$. We purposely opted for $St \leq 10$ regime, as studies on this regime are scarce. Moreover, $St \approx 1$ is often encountered in industrial applications, such as in pulverized coal burners (Nathan *et al.*, 2012), while particle clustering pattern also changes around $St \approx 1$. Additionally, particle dispersion characteristics with jet changes around *St* of unity. As the jet decays, the τ_c dwindles (u_c drops and $r_{1/2}$ increases as the jet evolves spatially). This causes the *St* of all the particles of both **H** and **NH** cases to drop below 0.5 (see Figure 1). Hence, all particle sizes are expected to behave as tracers by $x = 10$.

On the other hand, the initial fluid density is $\rho_{f,0} = 1$, and since $\rho_p/\rho_{f,0} \gg 1$, the only force experienced by the particles is the viscous drag force Maxey & Riley (1983). In $\rho_{f,0}$, the subscript 0 stands for the initial state of the variable. For simplicity, gravitational force is also neglected. After particle entrainment into the jet stream, particle heating is initiated after $x = 1$ for numerical stability. This is because, to rapidly heat the particles and transfer this heat to the local gas (required for the local viscous effects to be noticeable), we prescribed particle heating and particle-gas heat transfer timescales of $\tau_h = 1$ and $\tau_{th} = 4$, respectively, using the heating model of Mouallem & Hickey (2020). The local changes caused by the sharp rise in particle and gas temperature close to the inlet destabilized the simulations. The particles are heated until they reached a temperature of $T_p = 2$, after which the particle heating ceases and particles maintained their temperature.

Governing Equations

Gaseous Phase The nondimensional equations of mass, momentum and energy for the continuum phase are:

$$\frac{\partial \rho_f}{\partial t}+\frac{\partial \rho_f u_i}{\partial x_i}=0;\quad \frac{\partial \rho_f u_i}{\partial t}+\frac{\partial \rho_f u_i u_i}{\partial x_i}=-\frac{\partial P_f}{\partial x_i} + \frac{\mu_f \partial}{\partial x_j}\left(\frac{\partial u_i}{\partial x_j}+\frac{\partial u_j}{\partial x_i}-\frac{2\partial u_k}{3\partial x_k}\delta_{ij}\right)+F_p \tag{2}$$

$$\rho_f T_f \frac{Ds}{Dt} = \frac{\partial}{\partial x_i}\left(\kappa_f \frac{\partial T_f}{\partial x_i}\right) + 2\rho_f \nu_f S \otimes S + \zeta \rho_f \left(\frac{\partial u_i}{\partial x_i}\right)^2 + Q_{pf} \tag{3}$$

Here, μ_f, ζ, κ_f, P_f, T_f, S and Q_{pf} are gas dynamic viscosity, bulk viscosity, thermal conductivity, pressure, temperature, shear-rate tensor and particle-to-fluid heat transfer parameter, respectively. Here, temperature-driven gas dynamic viscosity is modeled with a power-law: $\mu_f = \mu_{f,0}\left(T_f/T_{f,0}\right)^{2/3}$. Here, $T_{f,0}$ is the initial gas temperature which is set to unity, and $\mu_{f,0} = \rho_{f,0}\nu_{f,0}$ is the initial gas dynamic viscosity which is prescribed as 0.001. This resulted in a flow Reynolds number of $Re = u_j d_j/\nu_{f,0} = 1000$.

Furthermore, the term $F_p = m_p\left(u_p - u_f(x_p)\right)/\tau_p$ in the momentum Equation (2) represents the particle back-reaction force. Here, u_p is the instantaneous particle velocity and $u_f(x_p)$ is the velocity of the gas in the vicinity of a particle, while m_p is the particle mass.

Particulate Phase The dimensionless Lagrangian equations for the point-particles are given as:

$$\frac{dx_p}{dt} = u_p;\quad \frac{du_p}{dt} = \frac{C_D}{\tau_p}\left(u_f(x_p) - u_p\right) \tag{4}$$

here, C_D stands for the particle drag coefficient (Carlson & Hoglund, 1964).

Results

It is emphasized that the thermodynamic difference in **H** and **NH** is fairly moderate. For example, the maximum rise in viscosity in **H** is about 16%, while it was 60% in the HIT case (Saieed & Hickey, 2024). Considering the evolution of *St* in Figure 6, similar particle clustering should be observed in the two simulations. Thus, even marginally higher clustering in the **H** case will suggest the strong influence of local rise in gas viscosity on particle clustering.

We first check if we get higher clustering in the **H** case compared to an identical **NH** simulation. For this purpose, we divided the domain into Voronoï cells and computed the probability density function (PDF) of the Voronoï cell volume (V), as shown in Figure 3. In this figure, the curves below the Gaussian curve on the left side depict clustering, while curves above the Gaussian curve on the right side depict voids. It is apparent that in the jet flow case, **H** particles are showing higher clustering, similar to the HIT studies. Note that our plot is different from the regular PDFs of Voronoï cell volume (Monchaux *et al.*, 2012). This is because in the jet flow case, there is a significant difference between the cell sizes in the domain since only the center region of the domain has particles, as shown in the 2D Voronoï tessellation diagram in Figure 4. This figure presents particle clustering in a slice of thickness $5\delta n_z$ at the center of the domain, where δn_z is the mesh cell size in the z-direction. Here we see that the **NH** particles portray the conventional trends where smaller particles disperse more and larger particles transverse along the centerline. Contrarily, the **H** particles are considerably more clustered, and also they are clustered at similar locations in the domain, irrespective of the size. This is highly non-intuitive and against the conventional behavior of inertial particles. We will elucidate this trend later in the present section. The observed rise in the

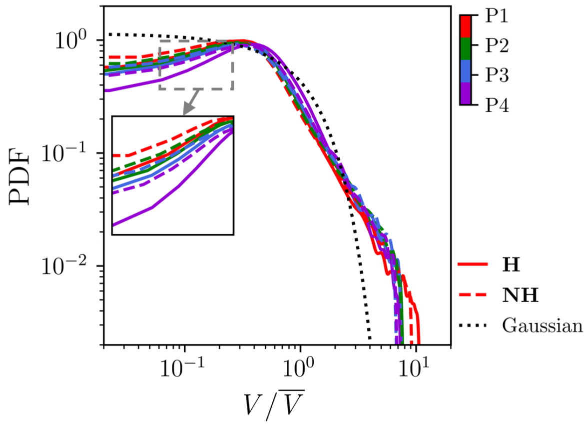

Figure 3. PDF of normalized Voronoï cell volume, where $\overline{V}$ is the mean volume of the all the cells. The V is computed by averaging Voronoï cell volume over 11 convective time units.

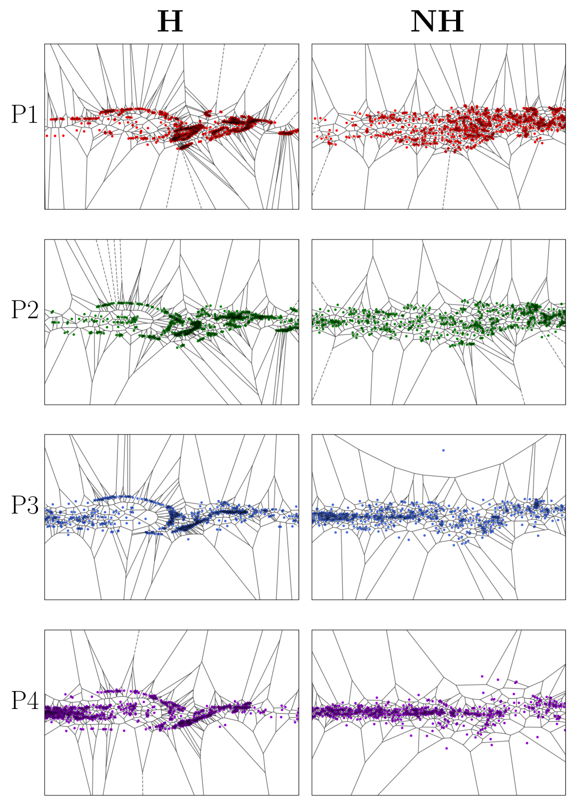

Figure 4. 2D Voronoï tessellation diagram of the **H** and **NH** particles at the center of the domain. The thickness of this slice is $5\delta n_z$.

clustering of **H** particles and their overall clustering pattern is surprising considering that the rise in fluid temperature causes the jet to spread, two-way momentum coupling enables particles to resist viscous effects and the local thermal effects are minimal as stated earlier. All of these aspects should nullify the effect of local viscosity driven clustering.

As shown in the 2D Voronoï diagram (Figure 4), the **H** particles are not spreading laterally according to the conventional trends. If this is true for the entire domain, then the **H** particles should show steeper decay in particle concentration in the lateral direction. This can be witnessed in Figure 5. Remarkably, the larger particles of the **H** case show less dis-

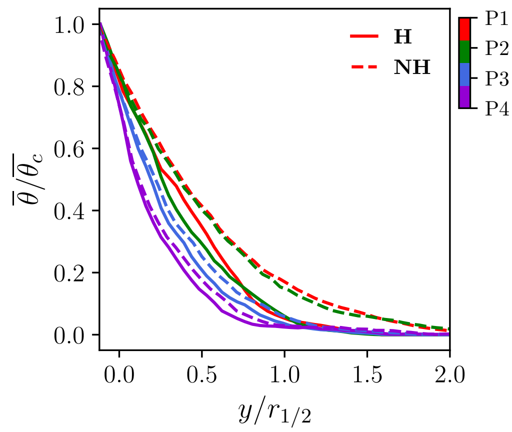

Figure 5. Mean radial concentration of particles ($\overline{\theta}$) normalized with the mean centerline particle concentration ($\overline{\theta_c}$).

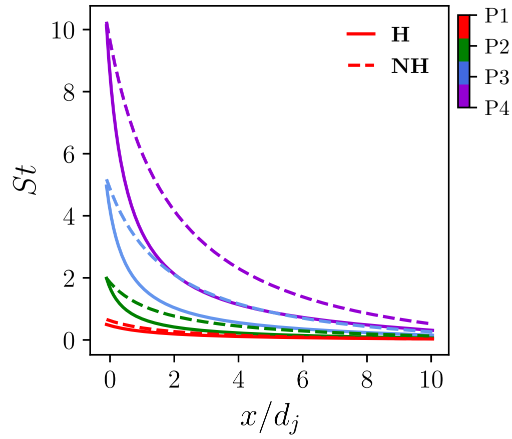

Figure 6. Time averaged axial evolution of the particle St.

persion than their **NH** counterparts, even though they are anticipated to disperse only slightly. The lower dispersion of the **H** particles further contains the thermal changes to the center of the domain, which can then causes more particles to remain within this region. We will elaborate this later in the present section. Note that both cases show the conventional trends where particle dispersion decreases with the increase in particles size. However, the **H** curves are steeper and closer to each other, signifying the effect of temperature-driven gas viscosity on particle clustering.

To understand the above stated trends, it is required to analyze the spatial evolution of the particle St in the domain, averaged over time. There is a chance that the St of **H** particles have evolved to a value of around unity, which might be the reason behind their higher clustering. For this, we plot the axial evolution of St in Figure 6, computed from the convective timescale (see Equation (1)). Since the St of the corresponding particles in the two cases start decaying from the same values, a similar clustering pattern should have been obtained even at later time instances, as per the *history* effect (Bragg & Collins, 2014). The sharp decline in the **H** curves is due to the rise in μ_f. There are a few key observations in this figure. Firstly, in the **NH** case, the curve of P3 overlaps with the P4 of **H**. Yet, the P4 of **H** show considerably higher clustering, see Figure 3. Furthermore, all four particle sizes of the **H** case start with different St values, but P1 to P3 show comparable

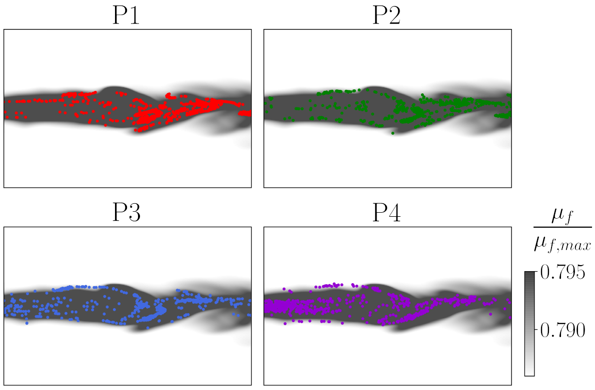

Figure 7. Contours of the high vorticity region of the jet overlaid with particles, in a thin slice of thickness $5\delta n_z$ at the center of the domain. The fluid viscosity is normalized with the fluid maximum dynamic viscosity, $\mu_{f,max}$.

clustering. The difference in clustering of the **H** particle sizes (Figure 3) can be attributed to the local viscous effects. For instance, the highest clustering of P4 of **H** can be elucidated with the fact that, viscosity-based enhancement in clustering primarily affects the particles that are well clustered prior to heating (Saieed & Hickey, 2024). As the P4 particles are located along the jet centerline before $x = 1$, they have a higher probability of forming clusters before heating. However, similar to HIT studies, the *St* based prediction of particle clustering does not hold. In the **NH** case, P3 and P4 show higher clustering because their *St* values approach unity as they travel.

Now that we have highlighted the disagreement between the particle clustering and *St*, the next question is, how is the rise in local viscosity augmenting particle clustering in a spatially evolving flow? To probe this, we present the contours of the high viscosity region of **H** simulation, overlaid with the scatter plot of particle position, in Figure 7. Here, all four particle sizes are present within the jet central region. The main reason behind this is, since particle are introduced within the jet diameter at the inlet, upon heating they cause the temperature/viscosity of the entire central region of the jet to increase. This bounds the particles within the jet via higher drag force. Residing within the jet, particles are exposed to the same large scale eddies as shown in Figure 8. This causes the particles to spread laterally. Yet, none of the particles are leaving the jet. This can be explained with the ability of particles to cluster at a thermal front (a location where a sharp scalar–temperature in this case–gradient exists (Bec *et al.*, 2014)). The particles experiencing higher lateral dispersion, encounter a thermal front as they approach the outer edge of the jet, and start clustering there. Since these particles cluster at the outer edge of the jet, they do not travel outside the jet. We can witness particles clustered at the outer periphery of the hot/high viscosity region of the jet in Figure 7. As a consequence of particle staying within the jet and encountering the same large eddies, particles in the **H** case are clustered at similar locations in the jet.

Next, it is expected that if the particles are staying inside the jet, the clusters formed in the **H** simulation should be more densely packed with particles. This can further aid the viscosity-driven rise in clustering. To quantify this, we employ the *Density Based Spatial Clustering of Application with Noise* (DBSCAN) (Ester *et al.*, 1996), which segregates the clustered and noise particles based on two parameters; inter-particle distance (D) and the minimum number of particles required to form a cluster ($N_{c,min}$). Here, $N_{c,min}$ is taken as twice the number of dimensions of the data (Sander *et al.*, 1998). In our case, particle location data are 3-dimensional, so $N_{c,min} = 6$. With the increase in D, the N_c should increase, and considering that the **H** particles are restricted in the jet, the number of **H** particles should increase much more rapidly than the **NH** particles. This trend can be seen in Figure 9. Hence, it is clear that particle heating and the consequent rise in local fluid viscosity can spatially restrict particles, which results in higher clustering.

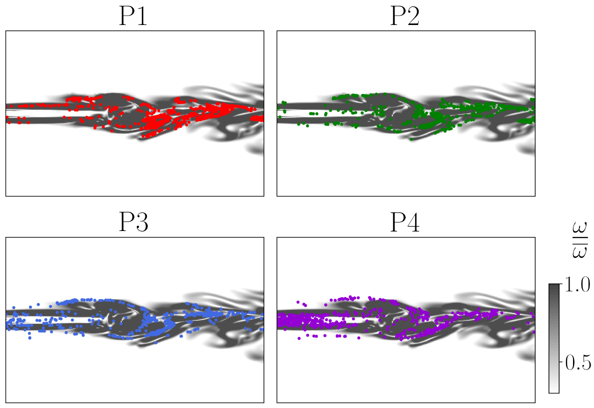

Figure 8. Contours of the normalized vorticity overlaid with particles, in a thin slice of thickness $5\delta n_z$ at the center of the domain. Here, $\overline{\omega}$ is the spatially averaged vorticity.

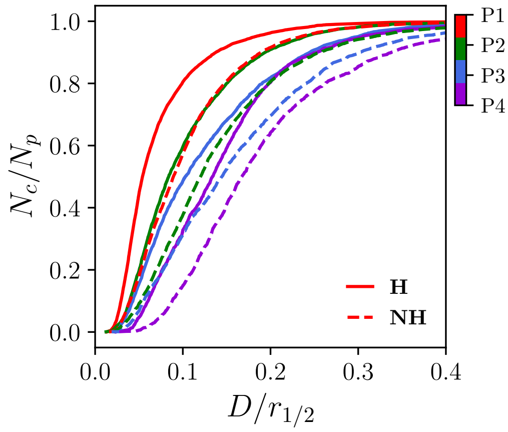

Figure 9. Number of clustered particles (N_c) versus the inter-particle distance (D), normalized with the total number of particles of each species (N_p).

Conclusions

We investigated the effect of temperature-dependent gas viscosity on heated particle clustering in a subsonic jet flow. By using direct numerical simulations, the particulate and continuum phases are modeled with the Lagrangian and Eulerian approaches, respectively. The temperature-driven gas viscosity is represented by a power-law. Despite the marginal difference between the heated and unheated simulations, a noticeably higher clustering is observed in the heated case. The introduction of particles within the jet caused the viscosity of the entire jet central region to increase. This caused the particles to stay within the jet via enhanced drag force, and even the particle reaction drag enabled by the two-way momentum coupling could not negate this effect. Additionally, this is a compounding phenomenon where the presence of particles at the center of the jet produces higher thermal changes at this location, which then further restricts the lateral movement of the particles. The particles present inside the jet face the same turbulent eddies, which cause them to disperse laterally. However, these laterally travelling particles are then clustered at the thermal front created at the outer edge of the jet. Hence, restricted within the same region, heated particles depict similar clustering regardless of their size. Albeit, both heated and unheated simulations started with identical initial conditions, had similar initial Stokes numbers, and the heating cases experienced a maximum of 16% higher viscosity, yet the concentration of the heated particles decayed steeply in the lateral direction, in comparison to the unheated particles. Thus, viscosity-based enhancement in particle clustering is found to be a surprisingly dominant phenomenon which prevails even in spatially and temporally evolving flows. This restricting ability of high viscosity jet can be beneficial to the fields of targeted drug delivery and advance manufacturing techniques such as cold sprays. However, it is detrimental to solid particle combustion in a jet.

Acknowledgement

This research is supported by the computational resources provided by SciNet, Sharcnet and Digital Research Alliance of Canada. Author Ahmed Saieed is funded by the NSERC Vanier graduate scholarship.

REFERENCES

Bec, J., Homann, H. & Krstulovic, G. 2014 Clustering, fronts, and heat transfer in turbulent suspensions of heavy particles. *Physical Review Letters* **112** (23), 234503.

Bragg, A. D. & Collins, L. R. 2014 New insights from comparing statistical theories for inertial particles in turbulence: I. spatial distribution of particles. *New Journal of Physics* **16** (5), 055013.

Brandenburg, A., Johansen, A., Bourdin, P. A., Dobler, W., Lyra, W., Rheinhardt, M., Bingert, S., Haugen, N. E. L., Mee, A., Gent, F. *et al.* 2020 The pencil code, a modular mpi code for partial differential equations and particles: multipurpose and multiuser-maintained. *arXiv preprint arXiv:2009.08231* .

Carlson, D. J. & Hoglund, R. F. 1964 Particle drag and heat transfer in rocket nozzles. *Aiaa Journal* **2** (11), 1980–1984.

Chung, J. N. & Troutt, T. R. 1988 Simulation of particle dispersion in an axisymmetric jet. *Journal of Fluid Mechanics* **186**, 199–222.

Crowe, C. T., Gore, R. A. & Troutt, T. R. 1985 Particle dispersion by coherent structures in free shear flows. *Particulate Science and Technology* **3** (3-4), 149–158.

Eaton, J. K. & Fessler, J. R. 1994 Preferential concentration of particles by turbulence. *International Journal of Multiphase Flow* **20**, 169–209.

Elghobashi, S. 1994 On predicting particle-laden turbulent flows. *Applied scientific research* **52**, 309–329.

Ester, M., Kriegel, H.-P., Sander, J., Xu, X. *et al.* 1996 A density-based algorithm for discovering clusters in large spatial databases with noise. In *kdd*, , vol. 96, pp. 226–231.

Hardalupas, Y., Taylor, A. M. K. P. & Whitelaw, J. H. 1989 Velocity and particle-flux characteristics of turbulent particle-laden jets. *Proceedings of the Royal Society of London. A. Mathematical and Physical Sciences* **426** (1870), 31–78.

Herman, H. & Sampath, S. 1996 Thermal spray coatings. In *Metallurgical and ceramic protective coatings*, pp. 261–289. Springer.

Hobosyan, M., Lyshevski, S. E. & Martirosyan, K. S. 2019 Integrated micropropulsion systems with nanoenergetic propellants. In *Nanomaterials in Rocket Propulsion Systems*, pp. 403–420.

Hussein, H. J., Capp, S. P. & George, W. K. 1994 Velocity measurements in a high-reynolds-number, momentum-conserving, axisymmetric, turbulent jet. *Journal of Fluid Mechanics* **258**, 31–75.

Lau, T. C. W. & Nathan, G. J. 2014 Influence of stokes number on the velocity and concentration distributions in particle-laden jets. *Journal of fluid mechanics* **757**, 432–457.

Li, M., Li, L., Zhang, B., Li, Q., Wu, W. & Zou, Z. 2020 Numerical analysis of the particle-induced effect on gas flow in a supersonic powder-laden oxygen jet. *Metallurgical and Materials Transactions B* **51**, 1718–1730.

Lodato, G., Domingo, P. & Vervisch, L. 2008 Three-dimensional boundary conditions for direct and large-eddy simulation of compressible viscous flows. *Journal of computational physics* **227** (10), 5105–5143.

Maxey, M. R. & Riley, J. J. 1983 Equation of motion for a small rigid sphere in a nonuniform flow. *The Physics of Fluids* **26** (4), 883–889.

Monchaux, R., Bourgoin, M. & Cartellier, A. 2012 Analyzing preferential concentration and clustering of inertial particles in turbulence. *International Journal of Multiphase Flow* **40**, 1–18.

Mouallem, J. & Hickey, J.-P. 2020 Induction heating of dispersed metallic particles in a turbulent flow. *International Journal of Multiphase Flow* **132**, 103414.

Nathan, G. J., Kalt, P. A. M., Alwahabi, Z. T., Dally, B. B., Medwell, P. R. & Chan, Q. N. 2012 Recent advances in the measurement of strongly radiating, turbulent reacting flows. *Progress in energy and combustion science* **38** (1), 41–61.

Poinsot, T. J. A. & Lelef, S. K. 1992 Boundary conditions for direct simulations of compressible viscous flows. *Journal of computational physics* **101** (1), 104–129.

Pouransari, H., Kolla, H., Chen, J. H. & Mani, A. 2017 Spectral analysis of energy transfer in turbulent flows laden with heated particles. *Journal of Fluid Mechanics* **813**, 1156.

Pouransari, H. & Mani, A. 2017 Effects of preferential concentration on heat transfer in particle-based solar receivers. *Journal of Solar Energy Engineering* **139** (2).

Rahman, M. M., Saieed, A., Khan, M. F. & Hickey, J.-P. 2022 Group combustion of dispersed spherical core–shell nanothermite particles. *Thermo* **2** (3), 209–231.

Saieed, A. & Hickey, J.-P. 2023 Viscous capturing of heated particles in one-and two-way coupled turbulence .

Saieed, A. & Hickey, J.-P. 2024 Viscosity-modulated clustering of heated bidispersed particles in a turbulent gas. *Journal of Fluid Mechanics* **979**, A46.

Saieed, A., Rahman, M. M. & Hickey, J.-P. 2022 Role of viscosity in the preferential concentration of heated, bidispersed particles. *International Journal of Multiphase Flow* **155**, 104185.

Sander, J., Ester, M., Kriegel, H.-P. & Xu, X. 1998 Density-based clustering in spatial databases: The algorithm gdbscan and its applications. *Data Mining and Knowledge Discovery* **2**, 169–194.

Squires, K. D. & Eaton, J. K. 1991 Preferential concentration of particles by turbulence. *Physics of Fluids A: Fluid Dynamics* **3** (5), 1169–1178.